PAPER

Low-threshold, nanosecond, high-repetition-rate vortex pulses with controllable helicity generated in Cr,Nd:YAG self-Q-switched microchip laser

IOP Publishing | Astro Ltd Laser Physics

Laser Phys. **28** (2018) 055802 (6pp) https://doi.org/10.1088/1555-6611/aaad4c

Low-threshold, nanosecond, high-repetition-rate vortex pulses with controllable helicity generated in Cr,Nd:YAG self-Q-switched microchip laser

Hong-Sen He, Zhen Chen, Hong-Bin Li and Jun Dong

Laboratory of Laser and Applied Photonics (LLAP), Department of Electronics Engineering, Xiamen University, Xiamen 361005, People's Republic of China

E-mail: jdong@xmu.edu.cn

Accepted for publication 6 February 2018
Published 21 March 2018

Abstract

A high repetition rate, nanosecond, pulsed optical vortex beam has been generated in a Cr,Nd:YAG self-Q-switched microchip laser pumped by the annular-beam formed with a hollow focus lens. The lasing threshold for vortex pulses is 0.9 W. A pulse width of 6.5 ns and a repetition rate of over 330 kHz have been achieved. The average output power of 1 W and the slope efficiency of 46.6% have been obtained. The helicity of the optical vortices has been controlled by adjusting the tilted angle between Cr,Nd:YAG crystal and output coupler. The work provides a new method for developing pulsed optical vortices for potential applications on quantum communication and optical trapping.

Keywords: beam reshaping, Cr,Nd:YAG, microchip laser, self-Q-switched laser, vortex beam, wavefront handedness

(Some figures may appear in colour only in the online journal)

1. Introduction

Since the orbital angular momentum was proved to be a natural character of all helically phased beams in 1992 [1], the vortex beam has been applied in sorts of fields, such as optical tweezers [2] and optical communications [3]. Vortex beams can be generated outside the laser cavity (passive methods) by making use of the spiral phase plate or digital micro-mirror device. However, the insertions of such optical elements result in the limitation of high power operation and degradation in beam quality, compared to the method of directly generating the vortex beam inside the laser cavity (active methods) [4, 5]. In active methods, the practical application of the vortex beam is determined by two key factors: the helical stability and laser power. The improvement of the two indexes will largely benefit the vortex laser performance in the end-pumped solid-state laser (EPSSL).

With regard to the helical stability, vortex pulses with stable helical wavefront are demanded in actual applications, such as the laser ablation [6], material-chirality control [7] and nonlinear frequency conversion [8]. Thus, it is crucial to investigate the mechanism of the wavefront handedness selection. Typical methods in EPSSL are adding mode-selecting elements in the laser cavity, such as the etalon [9], nanoscale stripes [10] and waveplate [11], to introduce loss differences for Laguerre–Gaussian (LG) beams with opposite handedness. However, the long cavity length is needed for the insertion of extra optical elements, which is not conducive to producing vortex beams with narrow pulse width and high repetition rate, according to the calculation of rate equations. Besides, the lasing threshold is increased owing to the insertion loss of extra elements in the laser resonator. For example, a black phosphorus plate was used in the laser cavity for Q-switching and controlling the handedness [12], and its pulse width was larger than 2.3 μs and repetition rate was lower than 40 kHz, and the lasing threshold for the absorbed pump power was estimated to be over 6 W. In the method of adding the etalon and acousto-optic Q-switch in the laser cavity [13], the pulse width increased with the repetition rate, and the obtained narrowest pulse width was 33 ns at 0.1 kHz. Therefore, a new

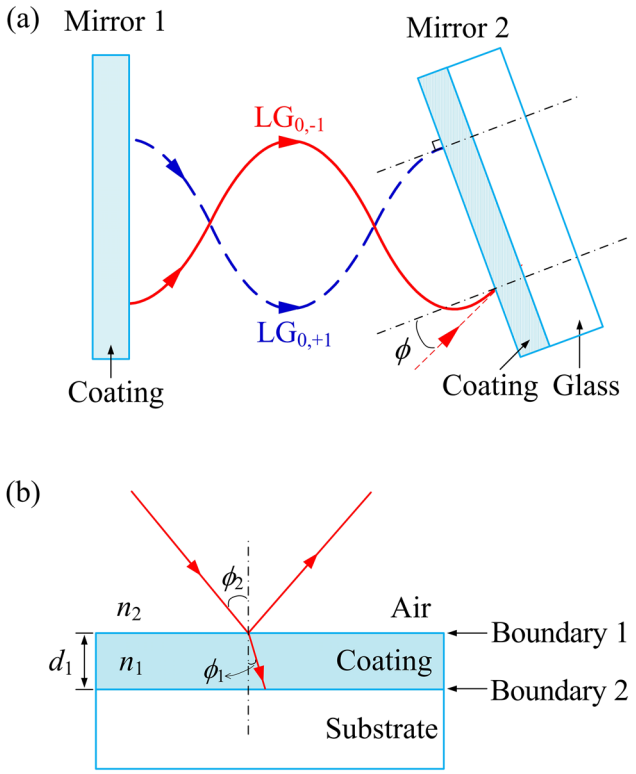

Figure 1. (a) Schematic diagram of enlarging the discrepancy of the reflectivity for intracavity vortex modes with opposite handedness based on controlling the tilted angle of the output coupler. The blue dashed and red solid lines denote the two helical propagation paths of $LG_{0,+1}$ and $LG_{0,-1}$ modes, respectively. (b) Geometric path of a light incident on a single film with a tilted angle.

method for controlling the wavefront handedness without adding additional optical elements in a compact laser cavity for the short pulse width and high repetition rate is needed.

In this paper, the switch of the wavefront handedness in a Cr,Nd:YAG self-Q-switched microchip vortex laser has been achieved based on controlling the tilted angle of the output coupler. There were no extra optical elements in the laser cavity for the handedness selection. The mechanism of the wavefront handedness selection in the microchip laser has been analyzed. The lasing threshold for vortex pulses was 0.9 W. To our best knowledge, it is the first time to simultaneously achieve the pulse width of 8.5 ns and repetition rate of 113 kHz at the low absorbed pump power of 1.8 W in EPSSL. The slope efficiency was up to 46.6% at higher pump power with the achievable average output power of 1 W. The laser spectra and polarization state of the output beam were also investigated.

2. Theory of wavefront handedness selection

Figure 1(a) shows the principle of controlling the wavefront handedness in a microchip laser by tilting the output coupler (OC). The composition of Mirror 1 and Mirror 2 forms the laser cavity. The coating of Mirror 1 totally reflects the laser beam, and the coating of Mirror 2 partly reflects the laser beam. According to [10], $LG_{0,+1}$ and $LG_{0,-1}$ modes would simultaneously oscillate in a symmetrical laser cavity of EPSSL due to the same lasing threshold when the annular pump beam was applied. The intensity distributions of the two vortex modes inside the laser cavity are the same, but the rotating directions of their spiral Poynting vector follow the symmetrical paths [9]. As shown in figure 1(a), the blue dashed and red solid lines denote the two helical propagation paths of $LG_{0,+1}$ and $LG_{0,-1}$ modes, respectively. For an intuitive description, the spiral paths are represented by the planar ones in figure 1(a). The reflectivity of Mirror 2 is determined by the thickness of its coating according to the principle of the optical coating. Thus, if the Poynting vector of the incident beam has an angle with Mirror 2, the reflectivity of the coating at the laser wavelength will be different with respect to the normal incidence. Figure 1(b) shows the geometric path of a light incident on a single film with a tilted angle. The amplitude reflection coefficient of a light incident on a single film [14] is expressed as

$$r = \frac{r_2 + r_1 \exp\left(-2i\delta_1\right)}{1 + r_1 r_2 \exp\left(-2i\delta_1\right)} \tag{1}$$

where $\delta_1 = 2\pi\lambda^{-1} n_1 d_1 \cos\phi_1$ and $n_2 \sin\phi_2 = n_1 \sin\phi_1$. r_2 and r_1 are the amplitude reflection coefficients at Boundary 1 and Boundary 2, respectively. n_2 and n_1 are the refractive indexes of the air and the coating, respectively. ϕ_2 and ϕ_1 are the beam incident angle and the refraction angle at Boundary 1, respectively. λ is the incident beam wavelength and d_1 is the thickness of the coating. According to equation (1), the change of incident beam angle ϕ_2 contributes to the variation of amplitude reflectivity r at a certain beam wavelength. In a normal laser resonator, the two cavity mirrors are parallel with each other, thus the propagation directions of $LG_{0,+1}$ and $LG_{0,-1}$ modes are always incident on Mirror 2 with the same angle, due to the constant symmetrical helical propagating paths of the two modes. Under this condition, the reflected beam intensities of the two modes by Mirror 2 are the same, thus with the same intracavity losses, the two modes will simultaneously emit and the output beam will have indistinguishable wavefront handedness. The undifferentiated wavefront handedness was shown in [10, 12]. However, when the OC is tilted, the Poynting vectors of $LG_{0,+1}$ and $LG_{0,-1}$ modes will have different incident angle at the boundary of the OC. As the situation in figure 1(a), the $LG_{0,+1}$ mode is perpendicularly incident on Mirror 2 while the $LG_{0,-1}$ mode is incident with an angle ϕ with Mirror 2. The intracavity loss of a Q-switched laser [15] can be expressed as

$$\text{Loss} = \frac{2\sigma_g N_g l_s + 2\sigma_e N_e l_s + \ln\left(\frac{1}{R}\right) + L}{2\sigma l} \tag{2}$$

where $R = |r|^2$, which is the intensity reflectivity. N_g is the ground state and N_e is the excited state population density of the saturable absorber (SA). σ_g and σ_e are the absorption cross-section of ground state and excited state of SA, respectively. σ is the stimulated emission cross section of the gain medium. l and l_s are the lengths of the gain medium and the SA, respectively. L is the non-saturable intracavity round-trip dissipative optical loss. According to equation (2), the increase of intensity reflectivity R results in the decrease of intracavity propagation loss. Therefore, due to the fact that the tilted OC contributes to different reflectivities for $LG_{0,+1}$

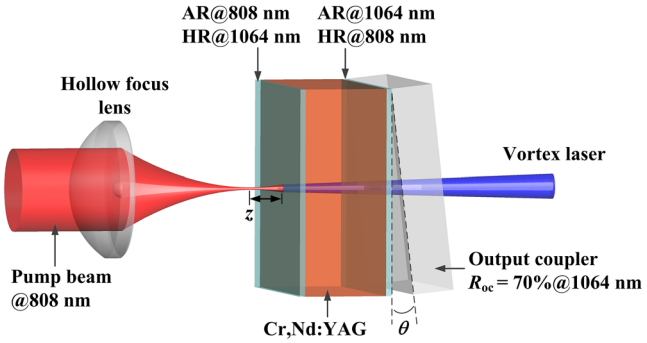

Figure 2. Experimental setup of a Cr,Nd:YAG self-Q-switched microchip laser for generating stable vortex pulses by tilting the output coupler.

and $LG_{0,-1}$ modes, oscillation intensities of the two modes inside the laser cavity are different. Concretely, the laser mode which is reflected more power by the OC will compete for more energy stored in the inversion population provided by the pump power, thus it will have a lower lasing threshold, while the other laser mode will be suppressed to oscillate due to the competition between transverse modes. Based on this principle, the wavefront handedness can be controlled in the microchip laser by adjusting the tilted angle of the OC. The main advantage of tilting the OC to control the wavefront is that this method utilizes its own component of the laser cavity, thus it makes the wavefront-handedness-switchable vortex laser more simple and compact, which is more conductive to producing vortex pulses with narrow pulse width and high repetition rate in EPSSL according to rate equations.

3. Experimental setup

The experimental setup of a Cr,Nd:YAG self-Q-switched microchip laser for generating stable vortex pulses by tilting the OC is shown in figure 2. The pump source was an 808-nm fiber-coupled laser diode. The output pump beam was collimated by a positive lens and then focused by a hollow focus lens (HFL), thus a focused annular pump beam was obtained behind the HFL focal point [16]. The focal lengths of the two lenses were both 8 mm. The gain medium was a 1.8 mm-thick Cr,Nd:YAG crystal, and it was doped with 1 at.% Nd^{3+} ions and 0.01 at.% Cr^{4+} ions. The coatings on one surface of the Cr,Nd:YAG crystal were the 808 nm antireflection (AR) and 1064 nm high reflection (HR), and it served as the rear mirror of the laser cavity. The coatings on the other surface were the 1064 nm AR and 808 nm HR. The reflection (R_{OC}) of the K9 output coupler was 70% at 1064 nm and the OC had an angle of $\theta = 0.5°$ with the Cr,Nd:YAG crystal. The tilted angle of the OC was determined by carefully adjusting the position of the reflected He–Ne laser point. The rear surface of the cavity was placed behind the HFL focal point and the distance was $z = 0.3$ mm. The incident pump beam on the rear surface of the laser crystal was in an annular shape with a measured beam diameter of 180 μm. The microchip laser was operated at room temperature without any cooling devices. The laser pulses were measured with a photodiode (5 GHz) and a digital oscilloscope (Tektronix, 6GHz, TDS6604). The laser spectra were observed with an optical spectral analyzer (Anritsu, MS9740A). The beam profiles were observed with a charge-coupled device (BC106-VIS, Thorlabs).

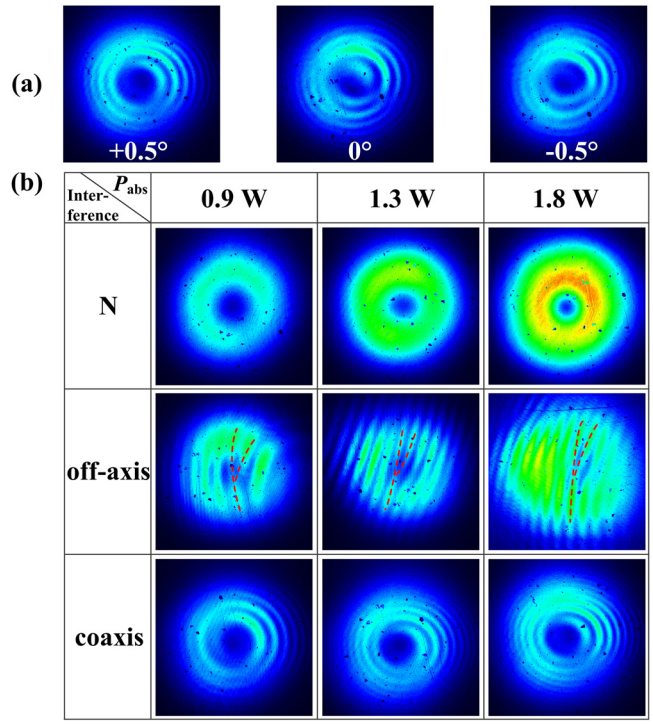

Figure 3. (a) Experimentally observed helical wavefront handedness under different tilted angle θ of the output coupler at $P_{abs} = 1$ W. θ is set to be $+0.5°$, $0°$ and $-0.5°$. (b) Annular transverse modes of the output laser beam at $P_{abs} = 0.9$, 1.3 and 1.8 W at $\theta = +0.5°$ and their corresponding interference patterns under off-axial and coaxial interference conditions. 'N' denotes the laser beam modes without being interfered.

4. Results and discussion

The theory of the wavefront handedness selection in passively Q-switched microchip laser is confirmed by the variation of the output beam wavefront state at different tilted angles of the OC. Figure 3(a) shows the experimentally observed helical wavefront handedness at different tilted angle θ of the OC under the absorbed pump power (P_{abs}) of 1 W. The plus and minus signs denote opposite rotating directions of OC. $\theta = 0°$ means the surface of the OC is parallel with the rear mirror of the laser cavity. As shown in figure 3(a), the wavefront of the output beam keeps the right handedness when the OC is tilted to $\theta = +0.5°$. It means the tilted OC contributes to more reflectivity for the right-handed vortex beam at $\theta = +0.5°$, while the left-handed vortex beam is suppressed to emit. When the OC is tilted to $\theta = 0°$, the output beam demonstrates an ambiguous wavefront handedness, which agrees with the theory that the two opposite handed vortex modes simultaneously oscillate with the same reflectivity provided by the parallel OC. When the OC is tilted to $\theta = -0.5°$, the wavefront of the output beam switches to the left handedness. The transition of the output wavefront handedness proves that the $LG_{0,+1}$ and $LG_{0,-1}$ modes can both oscillate in the laser

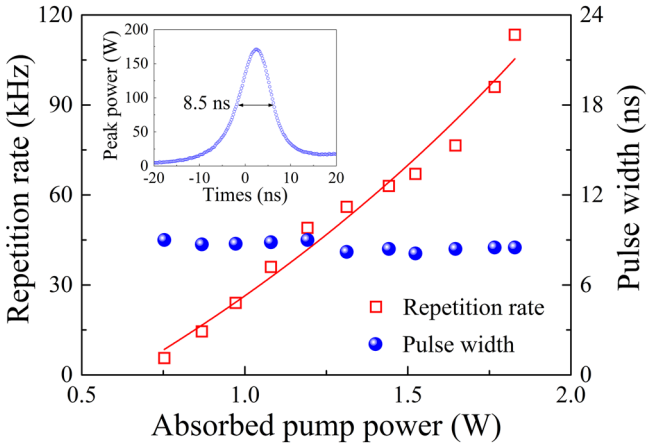

Figure 4. Repetition rate and pulse width of the output vortex laser beam as a function of P_{abs}. The solid line shows the variation tendency of the pulse repetition rate with P_{abs}. Inset: typical pulse profile of the Cr,Nd:YAG self-Q-switched microchip laser at $P_{abs} = 1.8$ W.

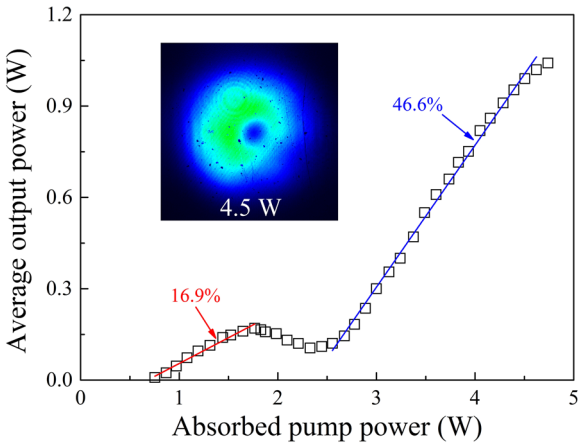

Figure 5. Average output power (P_{out}) of the Cr,Nd:YAG self-Q-switched microchip laser as a function of P_{abs}. Inset: laser transverse intensity distribution at $P_{abs} = 4.5$ W.

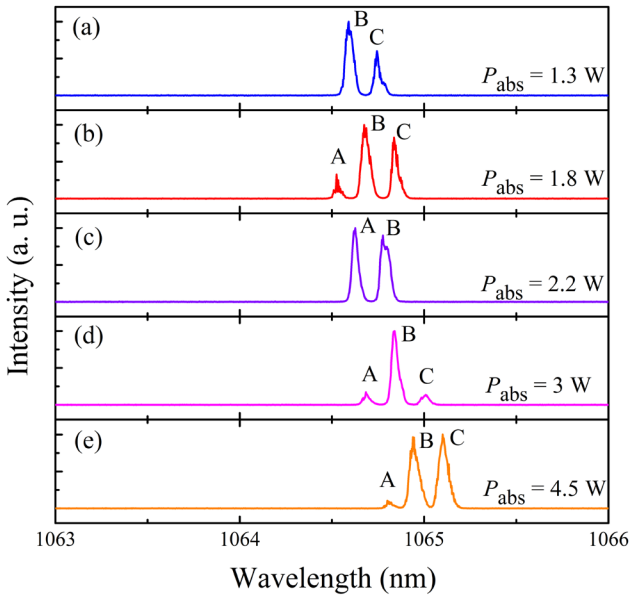

Figure 6. Laser emitting spectra of the Cr,Nd:YAG self-Q-switched microchip laser at different P_{abs}. 'A', 'B' and 'C' denote the three different longitudinal modes.

cavity, and by breaking the symmetry of the laser resonator, the pure vortex mode can be achieved.

By setting the tilted position of the OC at $\theta = +0.5°$, the laser performance of output vortex pulses in the Cr,Nd:YAG self-Q-switched microchip laser is investigated. Figure 3(b) shows the annular transverse modes of the output laser beam under different P_{abs} and their corresponding interference patterns. The lasing threshold was 0.75 W, and the $LG_{0,+1}$ mode was observed at $P_{abs} = 0.9$ W. With further increasing P_{abs}, the output laser beam remained the doughnut shape, as shown in the first row of figure 3(b). In addition, the annular transverse modes of the output laser beam were both coaxially and off-axially interfered with a spherical Gaussian beam to test the helical phase structure of the output beam. As shown in the second row of figure 3(b), the forklike interference patterns were observed under different P_{abs}. For all of the interference patterns, the single fringe splits into two at the fork dislocation, evidently confirming that the output laser beam possesses a phase singularity with the topological charge of $l = 1$. Moreover, the splitting directions of the forklike interference patterns are the same under the increasing pump power, which indicates that the output vortex laser keeps stable handedness independent of the pump power. The stable vortex state of the output beam was also confirmed by the coaxial interference patterns, as shown in the third row of figure 3(b). The output helical wavefront maintains the stable right handedness under the increasing pump power. The helical stability is mainly attributed to the microchip structure of the laser. When the intracavity-loss difference of the two vortex modes is set by the tilted OC, the robust structure of the monolithic self-Q-switched microchip laser guarantee the intracavity losses unchangeable; hence the output vortex laser beam keeps oscillating in the right handedness with further increasing pump power.

Figure 4 shows the repetition rate and pulse width of the output vortex laser as a function of P_{abs}. The repetition rate increases rapidly with P_{abs} and the repetition rate of 113 kHz is obtained at $P_{abs} = 1.8$ W. Compared with the maximum repetition rate of 41 kHz at $P_{abs} = 7.6$ W and 79 kHz at $P_{abs} = 6.5$ W achieved in the passively Q-switched lasers with black phosphorus [12] and graphene [17] as sturable absorbers respectively, the annular beam pumped self-Q-switched Cr,Nd:YAG microchip laser has the advantages of producing high-repetition-rate vortex beams at a rather low pump power. The high repetition rate achieved in this monolithic vortex laser is attributed to effective reduction of thermal effects of the laser materials due to the low pump power. As shown in figure 4, the pulse width keeps nearly constant with the increasing pump power and the shortest pulse width is 8.1 ns, which is achieved at $P_{abs} = 1.5$ W. As a comparison with the achievable pulse width of over 100 ns and the pulse repetition rate of lower than 10 kHz in the actively Q-switched Nd:YAG vortex laser by utilizing the acousto-optic Q-switch [18], the Cr,Nd:YAG self-Q-switched microchip laser is more suitable for generating short pulse width vortex pulses with high repetition rate. The inset of

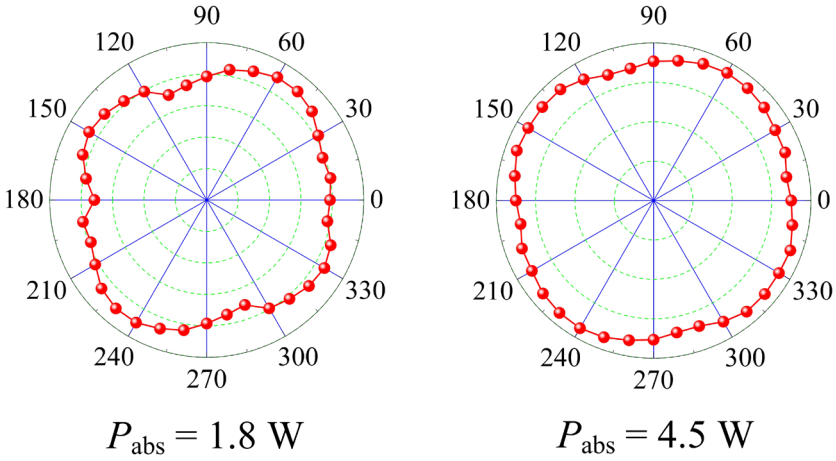

Figure 7. Polarization states of the output beam at $P_{abs} = 1.8$ and 4.5 W.

figure 4 shows the typical pulse profile of the Cr,Nd:YAG self-Q-switched microchip laser at $P_{abs} = 1.8$ W. The pulse width was measured to be 8.5 ns. The corresponding peak power was 171 W and the pulse energy was 1.5 μJ.

Figure 5 shows the average output power (P_{out}) of the Cr,Nd:YAG self-Q-switched microchip laser as a function of P_{abs}. In order to investigate the laser properties under higher pump power levels, the P_{out} under 1.8 W $< P_{abs} <$ 4.7 W was also measured. As shown in figure 5, the lasing threshold is 0.75 W. The P_{out} increases linearly with P_{abs} when $P_{abs} <$ 1.77 W, and the corresponding slope efficiency is 16.9%. The P_{out} of 170 mW is obtained at $P_{abs} = 1.77$ W. Then with further increasing P_{abs}, the P_{out} decreases with P_{abs} when $P_{abs} <$ 2.3 W. The P_{out} decreases to 105 mW at $P_{abs} = 2.3$ W. When $P_{abs} >$ 2.3 W, the P_{out} increases linearly with P_{abs}, and the slope efficiency is 46.6%, which is much higher than that under the low pump power. The P_{out} increases slowly and has a tendency to be saturated when $P_{abs} >$ 4.6 W. The maximum P_{out} of 1 W is achieved at $P_{abs} = 4.7$ W. The decline of the average output power of the pulsed vortex beam in the pump power range 1.8 W $< P_{abs} <$ 2.3 W is caused by the instability of the number of longitudinal modes in the laser cavity. Figure 6 shows the laser emitting spectra of the Cr,Nd:YAG self-Q-switched microchip laser under different P_{abs}. The output laser keeps oscillating in two longitudinal modes 'B' and 'C' when $P_{abs} <$ 1.77 W, as shown in figure 6(a), which contributes to the stable increase of P_{out} with the pump power. With further increasing P_{abs} up to 1.8 W, a third longitudinal mode 'A' emerges at the shorter wavelength, as shown in figure 6(b), competing for the energy with the previous two longitudinal modes. The competition for the energy among longitudinal modes becomes intense with further increasing the pump power, as the longitudinal mode 'C' is suppressed to oscillate at $P_{abs} = 2.2$ W, as shown in figure 6(c). Thus, during the pump power range 1.8 W $< P_{abs} <$ 2.3 W, the number of longitudinal modes is changeable, resulting in the unstable energy allocation among the longitudinal modes, hence accompanied by the temporary period of a lower optical conversion efficiency. When $P_{abs} >$ 2.3 W, a new balance of energy allocation is achieved owing to the fact that the energy provided by the pump power is sufficient to support the sustained oscillation of the three longitudinal modes 'A', 'B' and 'C', as shown in figures 6(d) and (e), therefore the P_{out} continues to increase linearly with the pump power.

The shape of the output laser beam tends to be a bit of distortion under higher pump power. As shown in the inset of figure 5, the intensity distribution of the laser transverse mode at $P_{abs} = 4.5$ W demonstrates an asymmetrical pattern, compared with the annular transverse modes under the lower pump power in figure 3(b). The beam quality degradation is attributed to the stress-induced birefringence in solid-state laser materials at the high pump power, which leads to the depolarization effect of the output linearly polarized beam [19]. Areas of high depolarization losses inside the laser cavity result in the intensity-descending parts of the output laser beam. At $P_{abs} = 4.5$ W, the repetition rate can be achieved up to 330 kHz while the pulse width is 6.5 ns. By taking advantage of the methods for alleviating the depolarization effect, the Cr,Nd:YAG self-Q-switched microchip laser can perform better in producing vortex pulses with narrower pulse width and higher repetition rate.

The polarization state of the output vortex beam was also measured. In this experiment, after the beam passing through the rotated polarizer, the beam profile kept the annular shapes with slight variations of the beam intensity. Figure 7 shows the polarization states of the output beam at $P_{abs} = 1.8$ and 4.5 W. At the two pump power levels, the polarization ratios were close to the circular polarization. Therefore, the output vortex beam was not vector polarized. The circular polarization state of the vortex beams obtained in the annular pumped Cr,Nd:YAG self-Q-switched microchip laser is different from the vector-polarized vortex beam observed in the Nd:YAG microchip laser [16]. The mechanism of circular polarized vortex beams in the annular-beam pumped Cr,Nd:YAG self-Q-switched microchip laser may be caused by the crystalline orientation selected nonlinear absorption of Cr^{4+} ions [20] and the further investigation is in progress.

5. Conclusions

A new method for controlling the handedness of the helical wavefront in a compact cavity of the end-pumped solid-state

laser was proposed based on adjusting the tilted angle of the output coupler. The mechanism of the wavefront handedness selection in the microchip laser is attributed to the different reflectivities for the intracavity vortex modes with opposite handedness provided by the tilted output coupler. This method realized the generation of low-threshold, nanosecond and high-repetition-rate vortex pulses with controllable helicity in a Cr,Nd:YAG self-Q-switched microchip laser. The lasing threshold for vortex pulses was 0.9 W. The pulse width of 8.5 ns and repetition rate of 113 kHz have been simultaneously achieved under the absorbed pump power of 1.8 W, and the slope efficiency of 46.6% was obtained under higher pump power with the achievable average output power of 1 W. The realization of the controllable helicity in the compact laser cavity with the significant improvement of laser performance contributes to high power and stable applications for vortex beams.

Acknowledgment

This work was supported by the National Natural Science Foundation of China (61475130 and 61275143), the Program for New Century Excellent Talents in University (NCET-09-0669), and the Fundamental Research Funds for Xiamen University (20720162005).

References

[1] Allen L, Beijersbergen M W, Spreeuw R J C and Woerdman J P 1992 Orbital angular momentum of light and the transformation of Laguerre–Gaussian laser modes *Phys. Rev.* A **45** 8185–9
[2] Grier D G 2003 A revolution in optical manipulation *Nature* **424** 810–6
[3] Bozinovic N, Yue Y, Ren Y, Tur M, Kristensen P, Huang H, Willner A E and Ramachandran S 2013 Terabit-scale orbital angular momentum mode division multiplexing in fibers *Science* **340** 1545–8
[4] Omatsu T, Miyamoto K and Lee A J 2017 Wavelength-versatile optical vortex lasers *J. Opt.* **19** 123002
[5] Lu J, Lin H F, Zhang G, Li B X, Zhang L Z, Lin Z B, Chen Y F, Petrov V and Dong C W 2017 Direct generation of an optical vortex beam from a diode-pumped Yb:$MgWO_4$ laser *Laser Phys. Lett.* **14** 085807
[6] Hamazaki J, Morita R, Chujo K, Kobayashi Y, Tanda S and Omatsu T 2010 Optical-vortex laser ablation *Opt. Express* **18** 2144–51
[7] Toyoda K, Takahashi F, Takizawa S, Tokizane Y, Miyamoto K, Morita R and Omatsu T 2013 Transfer of light helicity to nanostructures *Phys. Rev. Lett.* **110** 143603
[8] Strohaber J, Zhi M, Sokolov A V, Kolomenskii A A, Paulus G G and Schuessler H A 2012 Coherent transfer of optical orbital angular momentum in multi-order Raman sideband generation *Opt. Lett.* **37** 3411–3
[9] Kim D J and Kim J W 2015 Direct generation of an optical vortex beam in a single-frequency Nd:YVO_4 laser *Opt. Lett.* **40** 399–402
[10] Lin D, Daniel J M O and Clarkson W A 2014 Controlling the handedness of directly excited Laguerre–Gaussian modes in a solid-state laser *Opt. Lett.* **39** 3903–6
[11] Liu Q, Zhao Y, Zhou W, Zhang J, Wang L, Yao W and Shen D 2017 Control of vortex helicity with a quarter-wave plate in an Er:YAG ceramic solid state laser *IEEE Photonics J.* **9** 1–8
[12] Liu Q, Zhang B, Qi S, Li Y, Fan X, Zhao Y, Zhou W and Shen D 2016 Integration of helicity-control and pulse-modulation for vortex laser based on a black phosphorus plate *Opt. Express* **24** 30031–7
[13] Kim D J, Kim J W and Clarkson W A 2013 Q-switched Nd:YAG optical vortex lasers *Opt. Express* **21** 29449–54
[14] Heavens O S 1960 Optical properties of thin films *Rep. Prog. Phys.* **23** 1
[15] Dong J, Shirakawa A and Ueda K I 2005 Numerical simulation of a diode-laser-pumped self-Q-switched Cr,Yb:YAG microchip laser *Opt. Rev.* **12** 170–8
[16] He H S, Chen Z and Dong J 2017 Direct generation of vector vortex beams with switchable radial and azimuthal polarizations in a monolithic Nd:YAG microchip laser *Appl. Phys. Express* **10** 052701
[17] Ding Y, Xu M, Zhao Y, Yu H, Zhang H, Wang Z and Wang J 2014 Thermally driven continuous-wave and pulsed optical vortex *Opt. Lett.* **39** 2366–9
[18] Fang Z, Yao Y, Xia K and Li J 2015 Actively Q-switched and vortex Nd:YAG laser *Opt. Commun.* **347** 59–63
[19] Koechner W 1999 *Solid-State Laser Engineering* (Berlin: Springer)
[20] Eilers H, Hoffman K, Dennis W, Jacobsen S and Yen W 1992 Saturation of 1.064 μm absorption in Cr,Ca:$Y_3Al_5O_{12}$ crystals *Appl. Phys. Lett.* **61** 2958–60